

Absolute Flux Calibration of STIS Imaging Modes

Charles R. Proffitt,^{1,2} James Davies, Thomas M. Brown, Bahram Mobasher
Space Telescope Science Institute, Baltimore, MD 21218

Abstract.

The absolute flux calibration of STIS imaging photometry presents a number of unique challenges. The very wide wavelength coverage of most STIS imaging modes leads to significant color dependence in both the throughputs and the aperture corrections, complicating the determination of detector sensitivity. For CCD imaging modes, these difficulties are further complicated by the very broad scattered light halo at long wavelengths. For MAMA imaging modes, it is also necessary to take the time and wavelength dependent sensitivity changes of the detectors into account. We present deep imaging observations of a number of stars with well measured spectral energy distributions. These data have been used to derive improved color dependent aperture corrections for all STIS imaging configurations, and to revise the wavelength dependent detector sensitivities. These new aperture corrections and sensitivity revisions should allow absolute flux calibration of imaging observations with better than 5% accuracy for most STIS imaging modes.

1. Introduction

STIS has a small number of imaging modes for each detector, many of which have very broad bandpasses. Aperture corrections can be very large and strongly dependent on source color. Because STIS is also a well calibrated spectrograph, detailed wavelength dependent filter throughputs have been measured by taking slitless spectra through each filter. There remain, however, uncertainties in the overall wavelength dependent system throughput.

Our strategy is to calibrate the detector throughputs and encircled energy curves as a function of wavelength by obtaining very deep images of stars of a variety of colors and with well measured spectral energy distributions.

2. CCD Imaging Throughputs

Early STIS F28X50LP CCD images of several stars measured count rates 28% lower than expected, while 50CCD images of one hot star showed about the expected count rate. The initial response to this discrepancy was to lower F28X50LP throughput by 28%. However, this solution is not consistent with imaging results for cooler stars (e.g., Houdashelt, Wyse, & Gilmore 2001). Spectra taken through the F28X50LP filter also shows the throughput to be close to prelaunch estimates. The correct solution is to lower the long wavelength throughput of *all* STIS CCD modes and to properly measure the strongly color dependent aperture corrections.

¹Science Programs, Computer Sciences Corporation

²Catholic University of America Institute for Astrophysics and Computational Science

As part of STIS/CAL programs 8422, 8844, and 8924, we contained contemporaneous deep STIS 50CCD and F28X50LP images as well as STIS CCD spectra of a number of stars (Table 1) of a variety of colors. The deep images were used to derive color-dependent aperture corrections (Table 2), while the measured spectral energy distributions were used to adjust the CCD throughput curve (Figure 1) to obtain good agreement between predicted and measured imaging count rates (Figure 2).

In Table 1 we show the magnitudes and colors calculated for the CCD calibration stars using their observed spectral energy distributions and the currently adopted STIS component throughputs. Table 2 shows the measured aperture corrections for these stars.

Table 1. Calculated Magnitudes and Colors of CCD Imaging Calibration Stars in STMAG and VEGAMAG Systems

Star	STMAG			$UBVR_c$			
	50CCD	F28X50LP	50CCD-LP	V	$U - B$	$B - V$	$V - R_c$
GRW +70°5824	12.848	13.747	-0.899	12.716	-0.772	-0.057	-0.100
WD 310-688	11.603	12.361	-0.759	11.358	-0.624	+0.041	-0.079
CPD -60°7585	10.378	10.574	-0.196	10.041	-0.017	+0.417	+0.275
CPD -35°9181 A	10.402	10.328	+0.074	10.202	+0.833	+0.917	+0.583
BD -11°3759	10.318	9.994	+0.325	11.263	+1.241	+1.476	+1.274

Table 2. Measured Aperture Corrections for 50CCD and F28X50LP Images As a Function of the Aperture Radius in Pixels

Star	Aperture Radius in CCD Pixels (0.05071'')									
	2	3	4	5	7	10	15	19.7	39.4	59.2
50CCD										
GRW +70°5824	-0.464	-0.283	-0.219	-0.183	-0.137	-0.102	-0.074	-0.057	-0.021	-0.009
WD 310-688	-0.461	-0.276	-0.216	-0.194	-0.138	-0.105	-0.076	-0.060	-0.022	-0.010
CPD -60°7585	-0.523	-0.314	-0.242	-0.210	-0.169	-0.130	-0.104	-0.088	-0.043	-0.024
CPD -35°9181 A	-0.585	-0.352	-0.282	-0.244	-0.193	-0.152	-0.120	-0.102	-0.053	-0.029
BD -11°3759	-0.806	-0.524	-0.379	-0.328	-0.280	-0.235	-0.197	-0.173	-0.104	-0.064
F28X50LP										
GRW +70°5824	-0.621	-0.344	-0.245	-0.214	-0.166	-0.124	-0.094	-0.078	-0.036	-0.021
WD 310-688	-0.643	-0.363	-0.262	-0.228	-0.184	-0.140	-0.109	-0.091	-0.047	-0.026
CPD -60°7585	-0.632	-0.375	-0.288	-0.259	-0.215	-0.158	-0.127	-0.110	-0.059	-0.035
CPD -35°9181 A	-0.662	-0.397	-0.299	-0.273	-0.225	-0.182	-0.148	-0.126	-0.074	-0.039
BD -11°3759	-0.813	-0.535	-0.392	-0.346	-0.300	-0.251	-0.212	-0.187	-0.109	-0.068

Measurements and predictions (Table 3) are now in good agreement for stars of all colors (Figure 1).

3. MAMA Imaging Throughputs

Bright object limits prevent the usual WD flux standards from being observed with many MAMA imaging modes. Time dependent sensitivity changes are also important, especially for FUV MAMA imaging modes.

To calibrate the MAMA imaging throughput we use a strategy similar to that used for the CCD modes. For the narrow and some intermediate band MAMA filters we use STIS images and spectra of a number of WD standards from Bohlin, Dickinson, & Calzetti (2001). To calibrate the broad-band and intermediate imaging modes we use hot HB stars in the globular cluster NGC 6681 that were measured in STIS/CAL programs 8842 and 9631, and the star UIT1 in NGC 2808 (images are from STIS/CAL program 8511 and spectra from GO program 7436).

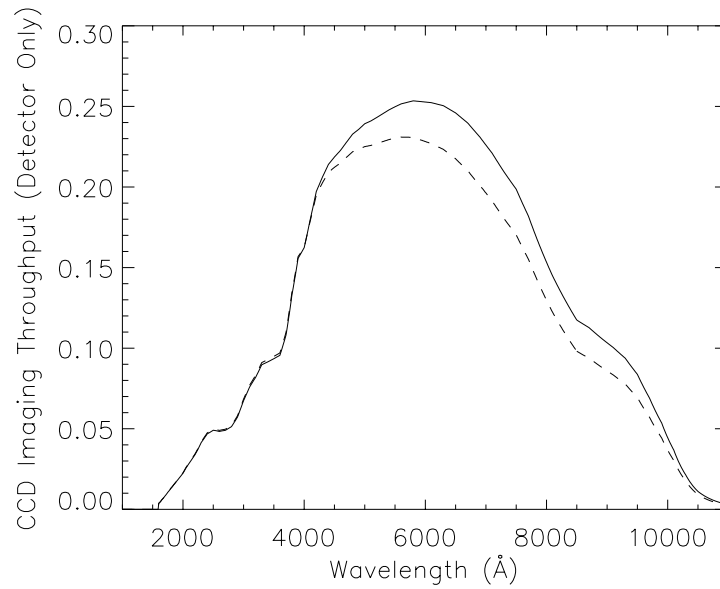


Figure 1. The old (solid line) and revised (dashed line) CCD throughputs are shown.

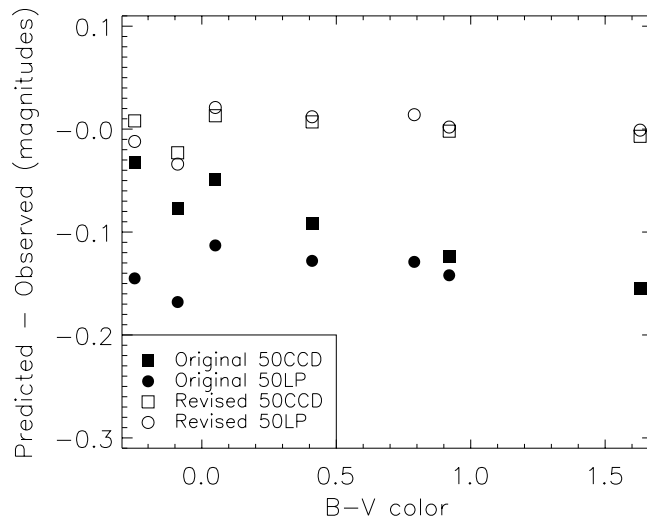


Figure 2. Here we compare the predicted and observed count rates for 50CCD (squares) and F28X50LP (circles) imaging of our standard stars for assuming the old (filled symbol) and the revised CCD throughputs (open symbols). For all calculated F28X50LP magnitudes in this figure, the revised F28X50LP curve is assumed.

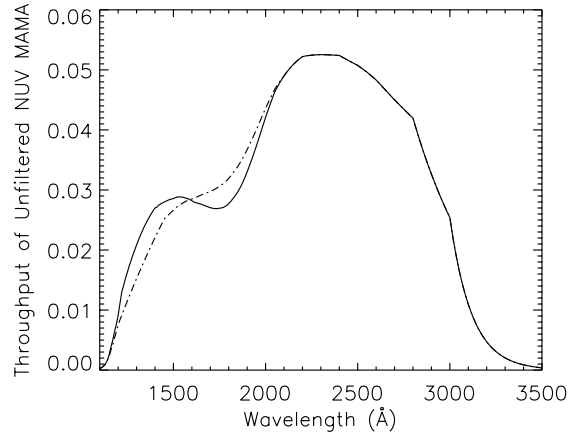


Figure 3. The solid line shows the throughput curve for NUV MAMA imaging modes adopted in July 1999. The broken curve shows our suggested revision. The throughput curves shown here have not yet been multiplied by the OTA throughput.

Wavelength dependant MAMA aperture corrections are based on the encircled energy curves from the deep imaging observations of individual stars.

For most detector/filter combinations, observations agree with predictions based on previously tabulated throughput curves to better than 5%. FUV F25QTZ observations show unusually large scatter, possibly due to long wavelength throughput variations across FUV MAMA. NUV MAMA F25CN182 observations are somewhat too bright compared with predictions. We have proposed a revision to the short wavelength throughput curve for NUV MAMA imaging modes (Figure 3) that alleviates this problem, and modestly improves the consistency of results for a number of other filters.

Table 3. Aperture Corrections for Individual MAMA Imaging Modes Calculated Assuming a Source Spectrum with F_{λ} =constant.

Detector/filter	Aperture Radius in MAMA Pixels (0.025")				
	3	5	10	15	20
NUV F25CIII	-0.680	-0.441	-0.287	-0.194	-0.130
NUV F25CN182	-0.664	-0.431	-0.279	-0.186	-0.123
NUV F25ND3	-0.561	-0.365	-0.223	-0.141	-0.093
NUV F25SRF2	-0.578	-0.375	-0.232	-0.149	-0.099
NUV F25QTZ	-0.572	-0.371	-0.230	-0.147	-0.099
NUV F25CN270	-0.512	-0.332	-0.198	-0.121	-0.082
NUV F25MGII	-0.485	-0.316	-0.182	-0.110	-0.073
FUV F25LYA	-1.030	-0.651	-0.381	-0.227	-0.127
FUV 25MAMA	-0.855	-0.556	-0.340	-0.214	-0.122
FUV F25ND3	-0.851	-0.554	-0.339	-0.214	-0.120
FUV F25SRF2	-0.785	-0.515	-0.323	-0.210	-0.120
FUV F25QTZ	-0.752	-0.494	-0.321	-0.218	-0.132

References

- Bohlin, R. C., Dickinson, M. E., & Calzetti, D. 2001, AJ, 122, 211
Houdashelt, Mark L., Wyse, Rosemary F. G., & Gilmore, G. 2001, PASP, 113, 49